The Cryosphere Discuss., 8, 2573–2610, 2014
www.the-cryosphere-discuss.net/8/2573/2014/
doi:10.5194/tcd-8-2573-2014

The Cryosphere Discussions
Open Access

Elevation changes of Inylchek Glacier during 1974–2007, Central Tian Shan, Kyrgyzstan derived from remote sensing data

D. Shangguan[1,2], T. Bolch[2,3], Y. Ding[1], M. Kröhnert[3], T. Pieczonka[3], H.-U. Wetzel[4], and S. Liu[1]

[1]State Key Laboratory of Cryospheric Science, Cold & Arid Regions Environmental & Engineering Research Institute, Chinese Academy of Sciences, Lanzhou 730000, China
[2]Department of Geography, University of Zurich, Zurich, Switzerland
[3]Institute for Cartography, Technische Universität Dresden, 01069 Dresden, Germany
[4]GFZ German Research Centre for Geosciences, Potsdam, Germany

Received: 31 March 2014 – Accepted: 30 April 2014 – Published: 21 May 2014

Correspondence to: D. Shangguan (dhguan@lzb.ac.cn)

Published by Copernicus Publications on behalf of the European Geosciences Union.

Abstract

Glacier melt is an important source of fresh water for the arid regions surrounding the Tian Shan. Inylchek Glacier (650 km^2) is the largest glacier in Tian Shan consisting of two branches (northern Inylchek glacier and southern Inylchek glacier) separated by the regularly draining Lake Merzbacher. However, little is known about volume and mass changes of the last decades. In this study, we investigated the changes of glacier area and glacier surface elevation from 1974 until 2007 and the surface velocity between 2003 and 2011 using multi-temporal remote-sensing data. The main flow direction of Southern Inylchek Glacier tongue showed strong velocities of $\sim 100\,m\,a^{-1}$ with a slight decreasing tendency between 2002/03 and 2010/11. The end of the tongue however, is likely stagnant as the main flow is directed towards Lake Merzbacher. The total glacier area increased by $1.3 \pm 0.1\,km^2$ ($\sim 0.2\,\%$) within the studies period though southern Inylchek Glacier shrank consecutive since 1974. The overall area gain was caused by the strong increase of northern Inylchek Glacier of $3.7 \pm 0.3\,km^2$ between 1990–1999. A comparison of glacier surface elevation using multi-temporal digital elevation models derived from KH9-Hexagon (1974), SRTM (1999), ALOS (2006) and SPOT5-HRG (2007) revealed an overall elevation difference of Inylchek Glacier of $-0.5 \pm 0.1\,m\,a^{-1}$ for the period of 1974–2007. The northern glacier branch showed on average no significant surface elevation change ($0.1 \pm 0.1\,m\,a^{-1}$) during 1974 and 2007 while a significant lowering of $0.7 \pm 0.1\,m\,a^{-1}$ was observed for the southern branch. The overall negative values are mainly due to the period 1974–1999. A possible thickening of $0.5 \pm 0.5\,m\,a^{-1}$ occurred between 1999 and 2007 where a clear thickening was measured in the accumulation area of the southern branch. We also identified the thickening with a maximum of about $\sim 150\,m$ close to the end of the northern Inylchek Glacier tongue for the period 1974–1999. This is possibly due to a surge event which happened between 1990 and 1999 according to the area change data. The ablation region of southern Inylchek Glacier showed considerable lowering rates especially in the distal part of the tongue with low velocity despite thick debris coverage.

1 Introduction

Meltwater from snow and ice is an important fresh water resource for the arid regions surrounding the Tian Shan (Sorg et al., 2012). This is especially true for the Tarim Basin in Xinjiang/Northwest China where current estimates report that about 40 % of the overall discharge of the Tarim River, the main artery for the very arid basin, is from glacier melt water (Aizen et al., 2007; Sorg et al., 2012), while the transboundary Asku River (named Sary-Djaz in Krygyzstan), originating in Central Tian Shan, contributes about 75 % to the overall run-off of Tarim River. On average, glaciers shrank also in this central region of Tian Shan but with lower rates than in the outer ranges (Sorg et al., 2012). Reported shrinkage rates vary between ~ 3.7 % for the entire Sary-Djaz Basin during 1990–2010 (Osmonov et al., 2013), and ~ 8.7 % for the neighbouring Ak-Shirak Range during 1977–2003 (Aizen et al., 2006). However, area changes show only indirect, filtered and delayed signals of climate change (Paterson, 1994). In addition, glaciers in Central Tian Shan are polythermal or even part of cold glaciers which have a lower mass turn over than temperate glaciers and, hence, lower changes in area than for temperate glaciers are typical. Only changes in ice thickness and mass balance can be more directly linked to climate and allow, taking the glacier area into account, direct comparisons with the climate reactions of other glaciers and regions and relate the changes directly to run-off. Glacier mass balance is traditionally measured in-situ. As this work is laborious and most of the glaciers are located in remote and hardly accessible terrain, measurements can only be conducted for few glaciers. Several studies have shown that remote-sensing derived geodetic mass balances are promising to extend the in-situ measurements and cover larger regions (e.g. Berthier et al., 2010; Gardelle et al., 2013; Paul and Haeberli, 2008). Most of these studies compare recent digital elevation models with the SRTM DEM from February 2000, while declassified and low cost stereo data from the 1960s and 1970s are only rarely used (e.g. Bolch et al., 2008; Pieczonka et al., 2013).

By using 1 : 25 000 scale topographic maps representing the glacier of the year 1977 and the SRTM DEM Aizen et al. (2006) presented an annual surface lowering of 0.69 ± 0.37 m a^{-1} for the Ak-Shyrak Massif while Pieczonka et al. (2013) found a mass loss of 0.43 ± 0.23 m a^{-1} using 1976 KH-9 data and the SRTM DEM for several debris-covered glaciers south of Jengish Chogsu (Pik Pobeda in Russian/Tomür Feng in Chinese). The loss was possibly lower in the period 1999–2009. Both clean-ice and debris-covered glaciers showed significant volume and mass losses. However, there is some spatial variability and even some rapid advancing and surging glaciers were found (Osmonov et al., 2013; Pieczonka et al., 2013; Aizen et al., 2006). Inylchek Glacier (IG), the largest glacier in Tian Shan which is investigated in this study is heavily debris covered at the tongue which alters both rates and spatial patterns of melting. IG was investigated both in the field (e.g. with ablation measurements, Hagg et al., 2008) and by remote sensing (especially for velocity measurements, e.g. Li et al., 2013). However, no information about the volume and mass changes are available until present.

In this work, we use 1974 KH9 Hexagon, 2006 ALOS, and 2008 SPOT5_HRG and the 2000 SRTM DEM to assess the volume change of IG by generating multi-temporal DEMs. In addition, we investigate area changes and the glacier flow using Landsat TM/ETM+ and Terra ASTER images.

2 Study region

Inylchek Glacier is located at the headwater of the Aksu-Tarim River catchment in the border triangle of Kyrgyzstan, Kazakhstan and China between Jengish Chogsu (Peak Pobeda/Tomur Feng, 7439 m a.s.l.) and Khan Tengri (6995 m a.s.l.), the highest peaks of the Tian Shan (Fig. 1). The glacier is stretching about 60.5 km with an area of approx. 650 km^2. It is the largest glacier of the Tian Shan and accounts for ~ 32 % of the total glacier area of the Sary-Djaz river basin (total ice cover: 2055 km^2 Ozmonov et al., 2013). The ELA is located at about 4500 m a.s.l. (Aizen et al., 2007). IG consists of two branches: northern IG and southern IG. Both branches are sepa-

rated by Lake Merzbacher which was formed due to the retreat of northern IG while the ice of southern IG forms and ice-barrier dams the meltwater (Häusler et al., 2011). Lake Merzbacher drains almost annually in summer/autumn causing an outburst flood which can well be measured 150 km downstream at the discharge measurement $1500\,m^3\,s^{-1} \sim 2000\,m^3\,s^{-1}$ in Xiehela hydrological station within Xinjiang/China (Ng et al., 2007; Glazirin, 2010). Existing velocity measurements of southern IG show surface velocities of about $100\,m\,a^{-1}$ for the middle part of the tongue of Southern IG. Interestingly the glacier flow is mainly directed towards Merzbacker Lake (Mayer et al., 2008; Nobakht et al., 2014).

13 % of the annual runoff during 1957–2006 in Aksu River was due to the glacier imbalance (Shen et al., 2009) and river runoff itself has likely changed as well (Li et al., 2008; Piao et al., 2012; Liu et al., 2006). Consequently, glacier-fed streamflow regimes have direct implications on freshwater supply, irrigation and hydropower potential which have brought serious problems to socio-economic development (Ng et al., 2007; Shen et al., 2009).

The area under investigation is characterized by a semi-continental climate. Precipitation recorded at Tian Shan station (1960–1997) (78.2° N, 41.9° E, 3614 m a.s.l.) and Koilu station (1960–1990) (70.0° E, 42.2° N, 2800 m a.s.l.) was $279\,mm\,a^{-1}$ and $311\,mm\,a^{-1}$, respectively (Reyers et al., 2013) with about 75 % occurring during summer. Hence, IG is mostly of summer-accumulation type (Osmonov et al., 2013). No longer-term precipitation measurement exists on the glacier itself and no information is available for the higher elevations. However, it can be estimated that the precipitation in the accumulation region is significantly higher than the measured values at these weather stations. The mean annual temperature is about −7.7 °C with January being the coldest month (−21.8 °C) and July the warmest (4.3 °C) (Osmonov et al., 2013).

3 Data and methods

3.1 Remote sensing datasets

Declassified Hexagon KH-9, SRTM Unfilled Finished-B version, SPOT5-HRV, ALOS PRSIM, Terra ASTER and Landsat TM/ETM+ data were used to obtain information about the surface elevation, surface velocity and area extent of IG for different periods (Table 1). The utilized data shall shortly be introduced in the following.

The KH9-Hexagon mission was part of the US keyhole reconaissance satellite program whose images were declassified in 2002 (Phil, 2013). The employed frame camera system was used on a total of 12 missions between 1973 and 1980. Each scene is characterized by a spatial resolution of about 20–30 feet (6–9 m) with 240 km × 120 km ground coverage. Due to the frame camera design (comparable to that of a Large Format Camera) Hexagon images are characterized by four fiducial marks and 1081 reseau crosses, which can be used to restore the image geometry at the time of image acquisition. For the KH9 missions the same film as for the KH4 mission with a film resolution of about 85 line pairs mm^{-1} was used. In our study we used Hexagon images from mission 1209 flown in November 1974.

During the Shuttle Radar Topography Mission (SRTM) the Earth's surface was measured by the use of two C-Band radar antennas in the period 11–22 February 2000. The SRTM data is available for free with a resolution of 3 arc-second (approximately 90 m). Yang et al. (2011) and Shortridge et al. (2011) reported an absolute vertical accuracy of the final DEM is about 10 m. However, the accuracy in mountain terrain is likely worse (Gorokhovich et al., 2006). The original SRTM dataset has some data voids especially at high elevation, mountainous regions due to radar shadow and layover effects. Thus, large parts of the accumulation region are not covered by the SRTM DEM. Meanwhile the gaps in the SRTM4 data were filled with auxiliary data. However, exact time is only known for the original data. We used the Unfilled Finished-B version with 3 arc-second resolution (USGS, 2006) for this study. Due to the acquisition in February 2000 glacier surfaces represent almost the end of the ablation period of

1999. The penetration of the C-band radar waves which will be 1–2 m on exposed ice, but can reach values up to 10 m on dry, cold firn (Rignot et al., 2001) needs to be taken into account.

SPOT5 was launched in May 2002 and is equipped with a High Resolution Stereoscopy (HRS) instrument and two High Resolution Geometrical (HRG) instruments. The HRS on SPOT5 offers the forward and backward view of the satellite in an along-track mode, provides panchromatic images with a ground sampling distance (GSD) of 10 m across and 5 m along the flight. The SPOT5-HRG instruments offer across-track stereo images with the viewing angle being adjustable through ±27° from two different orbits (Toutin, 2006). Due to the precise onboard measurements of satellite positions and attitudes of the SPOT5 orbit, each pixel in a SPOT5 image can be located on the ground with an accuracy of ±25 m on the 66 % confidence level without any ground control points (GCPs) (Bouillon et al., 2006; Berthier et al., 2007). We used images acquired on 5 February 2008 with an incidence angle of −9.79° and 24.94° offering a B/H about 0.63, which is suitable for DEM generation in high mountain areas (Toutin, 2009) (Table 1). SPOT 5 HRG has a smaller B/H and GSD than SPOT 5 HRS. Thus, SPOT 5 HRG is more suitable than the HRS for the extraction of DEM in the study area. The contrast on the glacier of the utilized imagery is suitable for DEM generation. Glacier surfaces represent almost the end of ablation period of 2007 due to the acquisition in February 2008, a similar seasonal acquisition time to the SRTM DEM.

ALOS was launched in January 2006, carrying the PRISM optical sensor with the capability to observe the Earth surface with a spatial resolution of 2.5 m. The sensor operated in a triplet mode, i.e. three independent optical sensors acquire 35 km wide images in forward, nadir and backward views in along-track direction (Takaku et al., 2004). The viewing angle of the forward and backward sensors have an inclination of ±23.8° from nadir to realize a B/H-ratio of 1.0 while the B/H-ratio of forward and nadir, and nadir and backward views are both 0.5 (Table 1). We used the nadir and backward images. The horizontal accuracy of geometrical models with a Rational Polynomial Coefficient (RPC) file (which contains information about the interior and exterior infor-

mation) can achieve an accuracy of better than 6.0 m (or 7.5 m in horizontal direction and 2.5 m in vertical direction) without any GCPs (Takaku et al., 2004; Uchiyama et al., 2008). This high accuracy can even be further improved by using precise GCPs.

In addition to the above mentioned imageries we used Landsat TM/ETM+ and Terra ASTER to investigate the changes in glacier extent and to observe the glacier flow (Table 1). Unfortunately only the southern branch was covered by the utilized ASTER scenes.

3.2 Glacier boundary

The glacier boundaries had to be delineated manually as both SPOT5 and KH9 are panchromatic images. Debris cover on the tongue of south IG made the accurate identification of the glacier margin difficult. However, water outlets from the southern IG tongue and the traces left after the river flow around the tongue are visible in the images. We identified the lines of demarcation of the traces surrounding the debris covered ice as glacier terminus boundary (Fig. 3a). For the northern IG terminus boundary the line of demarcation between the water and debris was used as the terminus boundary of ice (Fig. 3b). A hillshade calculated based on the SRTM DEM provided additional information to detect the glacier boundary. The accuracy of the glacier outlines is difficult to assess as appropriate reference data is not available for this glacier. Debris cover and spatial resolution are two key causes of uncertainty (Paul et al., 2013). We estimated the uncertainty using a buffer of 10 m for the Hexagon image (cf. Bolch et al., 2010) and half a pixel for Landsat TM/ETM+. This led to an uncertainty of the mapped northern IG area of about 2.7 %, 1.8 %, 1.3 %, 0.5 % and southern IG area of 1.9 %, 1.3 %, 0.9 %, 0.3 % for the Landsat TM, KH-9, Landsat ETM+ and SPOT5 images. The uncertainty of glacier area change is also evaluated considering the absolute change by using the buffer method (cf. Bolch et al., 2010). However, this uncertainty is probably upper bound because glacier area changes typically occur in the ablation region and we compared the absolute change in area. Finally, the uncertainties are 9.4 % between 1974–1990, 5.6 % between 1990–1999, 21.4 % between 1999–2007, 4.5 % between

1974–2007. The uncertainty is largest between 1999–2007 (21.4 %) due to the little absolute change in area.

3.3 Flow velocity of southern Inylchek Glacier

To investigate the dynamic behaviour of southern IG, we measured glacier velocity rates using optical satellite imagery covering a time span of about one year. Using the EXELIS VIS ENVI Add-on COSI-Corr a frequency based feature tracking (phase correlation) was performed in order to get the horizontal offset of corresponding image points. The relative offsets of the co-registered images feature the phase difference of the previously Fourier transformed input data and can be estimated by the correlation maximum (Leprince et al., 2007). For the 2010/2011 observation period offsets in north-south- and east-west-direction were measured with an accuracy of 1/7 px using quasi coregistered Landsat TM (L1T) data. For time period 2002/2003 we achieved a precision of 1/4 px based on 1/25 px-coregistered ASTER (L1A) data. As a final step a sound accuracy assessment has been performed. Uncertain classifications caused by clouds, topography and less image contrast have been removed from the matching result. This resulted in a threshold of significance of 0.25 m a^{-1} for 2002/2003 and 0.47 m a^{-1} for 2010/2011.

3.4 DEM generation and data coverage

Both ALOS PRISM and the SPOT5 HRG were processed using Leica Photogrammetric Suite (LPS), vers. 2011 with the UTM WGS84 reference system. Four GCPs in both ALOS and SPOT images were used to improve the accuracy of the exterior orientation. The reports of GCPs residuals are listed in Table 2. The automatically generated tie points (TPs) were visually checked to ensure accuracy. Overall, 120 TPs were used. The spatial resolution of the ALOS and SPOT5 DEM was chosen with 10 m.

Large parts of the accumulation region and more than 90 % of the glacier terrain with a slope larger than 15° are not covered by the SRTM DEM. The Hexagon DEM does

also have only about 7 % in the accumulation region. Considering that the accuracy of the DEMs on plane surfaces (slopes smaller 15°) is better than in mountain terrains evaluated by the State Bureau of Surveying and Mapping in China (SBSM, 2007), we only selected those region where slope is less than 15° as the study region. In addition, regions in SPOT5 DEM influenced by cast shadows were also eliminated from the final DEM. Considering the data gap in the accumulation region, it was not possible to properly calculate the mass balance of the glacier, but results on volume and elevation changes of the covered parts provide important insights into the glacier behaviour.

3.5 DEM postprocessing

Important for the calculation of the glacier volume changes based on two different DEMs is that they match relatively well to each other, hence possible horizontal shifts or vertical offsets are minimized (Nuth and Kääb, 2011; Pieczonka et al., 2013). Previous studies have shown that the bias of two DEMs of the same terrain surface has a sinusoidal relationship between elevation difference and aspect (Nuth and Kääb, 2011). We used the analytical method for co-registration based on the elevation difference and aspect developed by Nuth and Kääb (2011) which has been proven to provide robust results and is computational effective (Paul et al., 2014). All DEMs were bilinearly resampled to the same cell size of 30 m. The resolution is a compromise between the possible higher resolution of Hexagon and SPOT5 DEMs and the lower resolution of the SRTM DEM. The shift vectors were calculated based on selected ice free sample regions (Fig. 2). The resulting horizontal shifts were in the order of 1 pixel and the z-offsets varied between few meters and almost 20 m (Table 3).

3.6 Glacier elevation change and DEM uncertainty

The different DEMs were subtracted from each other to calculate the elevation differences (Fig. 4). Outliers identified by elevation difference values larger than 3σ are excluded in the calculation of elevation change (cf. Gardner et al., 2013; Gardelle et al.,

2013) between 1999 and 2007. For the northern IG between 1974 and 1999 and between 1974 and 2007, outliers were defined and excluded as follows: all values larger than the sum of the maximum elevation difference (which is larger than 3σ) in the surging region, standard deviation and mean of the elevation difference (Table 3). The biases of different DEMs in stable and no-glacierized regions after co-registration are shown in Table 3.

In order to consider the penetration of the SRTM C band signal, we compared the DEMs derived from the SRTM-C-band and SRTM-X- Band Synthetic Aperture Radar which both cover the IG. The result showed that the mean penetration depth varies between 1.7 m in the lower but debris-free ablation area and about 4.3 m in the higher accumulation area. We assume that there is no penetration in the debris-covered part of the glacier. The uncertainty of the radar penetration ($e$rp) was estimated to be 1.9 m.

The uncertainty of the DEM differencing was estimated by the normalized median absolute deviation (NMAD) in the ice free terrain which is assumed to be stable over time. Hence, the uncertainty of the DEM differencing will be calculated according to Eq. (1).

$$e = \sqrt{\mathrm{NMAD}^2 + e\mathrm{rp}^2} \quad (1)$$

In order to verify the accuracy of the DEMs, we also randomly collected six GPS points by using Uni-Strong GPS-RTK in situ surveys in 2010. Among the GPS points, three are in the debris covered region, 2 are in the glacier free region and one is in the glacier region (Table 4). The mean difference between GPS and SPOT DEM is −8.2 m with standard deviation 6.6 m before co-registration. After co-registration, it is −0.4 m with standard deviation 5.7 m. However, we cannot evaluate the bias of ablation in the debris covered region and the glacierized region between 2008 and 2010 and we also cannot evaluate the bias from the points by GPS in comparison to the DEMs cell size. In order to analyse the relative uncertainty of the ALOS DEM compared to the SPOT5 DEM we measure a profile with 342 sample points between 3050 and 3350 m a.s.l. on the glacier. The result showed that the uncertainty is 4.5 m with a standard deviation of

3.6 m. This uncertainty included the glacier melt and glacier elevation changes between 2006 and 2007.

The elevation change from DEM differences was calculated based on the area-weighted average per 100 m elevation zone (cf. Xu et al., 2013; Fomula 2).

$$\Delta h_{\mathrm{gl}} = \frac{\sum_{i=\mathrm{belt1}}^{n} \Delta h_i \times s_i}{s_{\mathrm{all\ zones}}} \quad (2)$$

where i is the number of zones, Δh_i is mean glacier elevation change in i zone after considering the radar penetration, s_i is the area of i zone, n is the total number of zones, and $s_{\mathrm{all\ zones}}$ is the area of overall zones. The distal part of the tongue of south IG which is not covered by the SPOT5 DEM (Fig. 1) was filled with the ALOS DEM. We used the elevation change per year as ALOS and SPOT5 were acquired at a different time.

4 Results

4.1 Glacier flow

We noticed high velocities with an average of about 120 m a^{-1} for the southern IG towards the Merzbacher Lake while the remaining part of the debris-covered tongue below the lake has significantly lower velocities with decreasing rates and is even partly stagnant (Fig. 3). Hence, the main flow direction of the tongue is towards Lake Merzbacher and not to the end of the glacier tongue. Most tributaries have active flow until the confluence of the glacier with velocities varying typically between 30 and 60 m a^{-1}. The general patterns and velocities are similar for both investigated periods (2002/03 and 2010/11). There is a slight decrease in velocity especially for the southern tributary glaciers.

4.2 Glacier area change

Southern IG shrank continuously by about 0.1 km^2, 0.5 km^2 and 0.2 km^2 during the periods 1974–1990, 1990–1999, and 1999–2007. The overall area loss of southern IG was 0.8 ± 0.1 km^2 during 1974 and 2007, accounting for ~ 0.2 % of its area in 1974. Northern IG lost an area of 1.2 ± 0.1 km^2 during the period 1974–1990 followed by an increase in area of 3.7 ± 0.3 km^2 (1990–1999). During this period the glacier showed a strong advance of about 3.5 km. The glacier shrank again by 0.4 ± 0.1 km^2 in the consecutive period (1999–2007). Overall, the area of northern IG increased by 2.0 ± 0.1 km^2 during 1974–2007, accounting for ~ 1.3 % of its area in 1974 (Fig. 4; Table 5). Consequently, the area of the two branches of IG increased by 1.3 ± 0.1 km^2 (~ 0.2 %) between 1974 and 2007.

4.3 Glacier elevation change

On average, the investigated parts of IG thinned by -0.5 ± 0.1 m a^{-1} during 1974 and 2007 (Table 6). However, for the recent period (1999–2007) we found a slight thickening of 0.6 ± 0.5 m a^{-1}. The overall thickening is mainly due to a thickening in the higher elevations above 4000 m a.s.l. in the accumulation zone while there was a slight lowering at the distal parts of the tongue (Fig. 6). Between 1974 and 1999 a significant surface lowering was observed by -0.8 ± 0.1 m a^{-1}. Northern IG showed on average no significant surface elevation change (0.1 ± 0.1 m a^{-1}) during 1974 and 2007 while a significant lowering of 0.7 ± 0.1 m a^{-1} was observed for southern IG. The significant difference is due to the period 1974 to 1999 when a strong thickening of 0.7 ± 0.1 m a^{-1} of northern IG was observed (Table 5). Taken the strong advance between 1990 and 1999, it can, hence, be assumed that northern IG was surging during this period. After 1999 a slight thinning by 0.2 ± 0.5 m a^{-1} was measured for the northern IG while southern IG showed thickening by 0.5 ± 0.5 m a^{-1}. However, both northern and southern IG retreated between 1999 and 2007.

The analysis of the vertical changes (Fig. 6) in different elevation zones and along the main flow line (Fig. 7) for southern IG and northern IG allow more detailed insights into the characteristics of the behaviour of the glacier. Almost all parts of southern IG tongue which is covered by the DEMs showed a surface lowering for the periods 1974–1999 and 1974–2007 while there was no significant elevation change in the upper parts of the glacier for 1999–2007 (close to point a, Fig. 7). Interestingly, there are large amplitudes in elevation change between point c and point b (Fig. 7) which is the heavily debris-covered part below Lake Merzbacher with low flow velocities (Fig. 4). On average, the elevation change was 0.4 ± 0.1–0.6 ± 0.1 m a^{-1} below an altitude of 3200 m a.s.l. for the period 1974–1999 and 0.5 ± 0.1–0.6 ± 0.1 m a^{-1} below an altitude of 3400 m a.s.l. for the period 1974–2007 (Fig. 6). Between point b and a, a clear surface lowering could be observed for 1974–1999 and 1974–2007 while no significant surface elevation changes or even a slight increase could be measured considering the 1999–2007 period only (Figs. 5–7); between the altitude of 3400–4000 m elevation thinning varied between 0.2 ± 0.1 and 1.4 ± 0.1 m a^{-1} m for the period 1974–1999 and 0.3 ± 0.1–1.2 ± 0.1 m a^{-1} for the period 1974–2007. This phenomena is similar with West Qongterang Glacier where a surface lowering occurred in the upper part of the ablation region (Pieczonka et al., 2013). We also identified that most of the elevation changes are positive above altitude $\sim$ 4000 m (point a) for 1999–2007 (Fig. 6). Above this altitude a surface lowering was measured for the period 1974–1999 (Fig. 6) while an elevation increase was measured for the period 1999–2007. However, the overall trend is still negative for the entire investigation period.

Northern IG showed a different behaviour. A clear thickening of more than 100 m was observed at the glacier tongue for the period before 1999 while a slight thinning of $\sim$ 15 m was measured thereafter. We noticed a maximum thickening of $\sim$ 150 m between 3300 and 3600 m a.s.l. in the period 1974–1999 (Figs. 6 and 7), while a section of the upper part ($\sim$ 9 km from the terminus) has clearly lost mass. The upper part is not covered by the Hexagon scene and that is why it is not possible to show the expected process of mass transfer during the glacier surge. After the surge event between 1999

and 2007 the covered part of the glacier tongue showed a mean thinning of $1.7 \pm 0.5\,\mathrm{m\,a^{-1}}$ (Fig. 7) while a thickening is visible ∼ 18 km from the terminus above 3900 m elevation zones (Figs. 5–7).

5 Discussion

Osmonov et al. (2013) reported an average shrinkage of 3.7 ± 2.7 % from 1990 to 2010 with 10 advancing glaciers in the upper of Aksu catchment. The glacier retreat in adjacent regions during the last decades varied between 3.3 % to ∼ 30 % (Bolch et al., 2007; Aizen et al., 2006; Liu et al., 2006) with highest shrinkage rates in the outer and more humid ranges and the lowest in the inner and drier ranges (Sorg et al., 2012; Narama et al., 2010). In western China including the Chinese Part of the Tian Shan more than 80 % of the glaciers were in retreat with some glaciers in an advancing phase (Ding et al., 2006). Our study revealed only a slight retreat of southern IG for 1974 and 2007 while a strong advance for northern IG between 1990 and 2000 could be identified. Our result is in tendency in agreement with Osmonov et al. (2013). However, the authors considered southern and northern IG including Lake Merzbacher as one glacier, the overall value was different and the surge was not detected.

Our observed flow characteristics of southern IG is in good agreement with the existing information (Nobakht et al., 2014; Li et al., 2013) for similar years. The observed velocity of $\sim 120\,\mathrm{m\,a^{-1}}$ for the main tongue is close to the measurements by Nobakht et al. (2014) who reported values of 0.3–0.4 $\mathrm{m\,day^{-1}}$ (~ 100–$150\,\mathrm{m\,a^{-1}}$) calculated based on ASTER and Landsat data but larger than $0.2\,\mathrm{m\,day^{-1}}$ ($\sim 75\,\mathrm{m\,a^{-1}}$) as obtained by Li et al., 2013) based on ALOS PALSAR data. Mayer et al. (2008) also measured velocity rates of up to 80–90 $\mathrm{m\,a^{-1}}$ closer to the lake in the period 2003/2004 which is in good correspondence with our velocity measurements of 75–90 $\mathrm{m\,a^{-1}}$ (0.2–0.4 $\mathrm{m\,day^{-1}}$) in the observation period 2002/2003 for the similar area. High velocities will transport mass from upstream and offset the mass loss due to the ice melt. Consequently, there was no ice lowering in southern IG between the length of 18 and 30 km

(Fig. 7) for 1999–2007. Glacier calving could be observed for southern IG with mean velocities of up to $0.4\,\mathrm{m\,day^{-1}}$ between 2009 and 2010 (cf. Fig. 5c) (Nobakht et al., 2014). This means that the presence of glacier dammed lakes is influencing the ice dynamics (cf. Mayer et al., 2008) and the mass change of a glacier.

Existing in-situ mass balance measurements in the Tian Shan showed clearly negative values since the beginning of the measurements in the 1960s (WGMS 2013; Sorg et al., 2012) and studies based on GRACE and ICESat laser altimetry data (Jacob et al., 2012; Gardner et al., 2013) pointed out that on average glaciers in the Tian Shan underwent clear mass loss between 2003–2009 but with a lower rate compared to the observed in-situ data. Geodetic mass balance measurements of 12 mainly debris-covered glaciers south of Pik Pobeda/Tomur Peak close to our study area revealed that most of the glaciers have been losing mass with rates between $-0.08 \pm 0.15\,\mathrm{m\,w.e.\,a^{-1}}$ and $-0.80 \pm 0.15\,\mathrm{m\,w.e.\,a^{-1}}$ for the time period 1976–2009. However, two glaciers gained mass and one glacier (Qingbingtan Glaicer No.74) showed signs of a surge similar to northern IG (Pieczonka et al., 2013). The mass loss was lower during the last decade (1999–2009) than during 1974 and 1999. This tendency is in line with our results for IG where a glacier thinning was found during 1974–1999 with strong thickening between 4400 and 5300 m a.s.l. followed by non-significant elevation changes between 1999 and 2007 (Fig. 5). Unfortunately, the data coverage above an altitude larger than 4000 m a.s.l. is less than 10 % of the glacier area for the periods 1974–1999 and 1974–2007 due to Hexagon KH-9 coverage which hampered to investigate the overall glacier's elevation change and assess the glaciers mass balance. In order to estimate the mass change of entire southern IG mass balance we assumed different scenarios to fill the data gaps: on the one hand no elevation change and on the other hand a thickening of the mean elevation change value of the covered parts of the accumulation region (13 m) for period 1999–2007. The mass balance values vary between 0.28 and $0.60\,\mathrm{m\,w.e.\,a^{-1}}$ assuming a density of $850 \pm 60\,\mathrm{kg\,m^{-3}}$ for the conversion of the volume to mass changes (cf. Huss, 2013). This indicates a positive mass balance for this time period. However, the mass balance since 1974 and especially for 1974–

1999 was clearly negative. Even assuming a large span of possible elevation changes in the non-covered areas between −20 and 20 m would not significantly alter the mass budget: the values are between −0.60 and −0.42 m w.e. a^{-1} for the period 1974–2007 and −0.73 and −1.00 m w.e. a^{-1} for 1974–1999. The data gaps are even larger for northern IG so that a suitable mass balance estimate is not possible. However, the obtained characteristics for the surface elevation change with a clear thickening at the tongue and a lowering in higher reaches (Fig. 6) together with the data of area and length change are a clear indicator for a surge event that happened between 1990 and 1999 Surging glaciers in the Tian Shan were also reported by Narama et al. (2010), Osmonov et al. (2013), Pieczonka et al. (2013) and, for earlier times, by Dolgushin and Osipova (1975), hence this phenomenon is also in the Tien Shan not infrequent. The surge event of northern IG described by Mavlyudov (1998) probably happened in late 1996 with an advance of about two kilometres (Häusler et al., 2011). However, it was a non-typical surging event due to the lack of surge characteristics such as areas of stretched ogives, erosion scars, transverse crevasses or breaching structures; Hodkins et al. (2009) described this phenomenon as partial surges. Cuffey and Paterson (2010) pointed out that mass displacement down-glacier is an important signal that occurs before a glacier surge. This result also showed that glacier surging will re-distribute the glacier mass.

Both of parts of ablation regions of southern IG and northern IG are covered by debris below ∼ 3500 m a.s.l. The surface of southern IG showed considerable lowering rates but also great variability for the time period of 1974–1999 and 1974–2007. The surface lowering is higher at the frontal part of southern IG where low flow velocity is measured. This is in line with several other studies which found significant mass loss despite thick debris cover (Bolch et al., 2011; Kääb et al., 2012; Nuimura et al., 2012; Pieczonka et al., 2013). Field based measurements in 2005 of moraine thickness and the ablation rates on southern IG revealed nevertheless a dependency upon debris thickness with ablation rates from 2.8 to 6.7 cm day^{-1} with a mean of 4.4 cm day^{-1} (Hagg et al., 2008). The lower velocities and even stagnancy of the part southern IG

tongue below the Lake Merzbacher indicates that there was little mass supplied from upstream. Therefore, the significant mass loss can be explained by the influence of backwasting at ice cliffs and melting at supraglacial ponds (Fujita and Sakai, 2010; Han et al., 2010; Juen et al., 2014) but likely also due to reduced glacier flow from the accumulation region and englacial conduits (Quincey et al., 2009; Schomacker, 2008; Benn et al., 2012).

Measurements at the Tian Shan station (3614 m a.s.l.) located 120 km west of IG suggested that both increasing temperature and decreasing precipitation were detected during the ablation season (May–September) for the period 1970–1996; and a decreasing temperature and slight decreasing precipitation was found also in the ablation season for the period of 1997–2009 (Osmonov et al., 2013). Hence, the observed glacier thinning between 1974 and 1999 is most likely a consequence of the ablation season warming and precipitation decreasing which led to an accelerated melting and decelerated accumulation. Reduced mass loss or even the possible balanced condition between 1999 and 2007 could be explained by the temperature decrease.

6 Conclusion

We investigated the velocity, glacier area and surface elevation changes of Inylchek Glacier from 1974 to 2007 based on various space-borne data such as KH9 Hexagon, Landsat and SPOT5 HRG data. Our results show that southern IG has a velocity of about 100 m a^{-1} for large parts of the tongue with a main flow direction towards Lake Merzbacher and low velocity with stagnancy at the terminus below the lake. The glacier shrank slightly during the time of 1974, 1990, 1999 and 2007; while northern IG was surging between 1990 and 1999 which caused an overall area increase of both branches of IG of 1.3 ± 0.1 km^2 (∼ 0.2 %) between 1974 and 2007 despite a shrinking of northern IG before 1990 and after 1999. The generated DEMs from 1974 and 2007 were of good quality for most glacier parts and allowed to calculate the volume changes along with the SRTM DEM. However, only parts (∼ 10 %) of the accumulation regions

were covered hindering to assess the mass balance for the entire IG. The tendency is clear nevertheless: a thinning of southern IG of $-0.8 \pm 0.1\,\mathrm{m\,a^{-1}}$ for the period of 1974–1999 was followed by a possible thickening of $0.5 \pm 0.5\,\mathrm{m\,a^{-1}}$ for 1999–2007 with an overall elevation difference of $-0.5 \pm 0.1\,\mathrm{m\,a^{-1}}$ for the entire period of 1974–2007 despite thick debris cover. The lowering is highest at the distal part of the tongue with low velocity. A clear thickening of up to $\sim 150\,\mathrm{m}$ was found for northern IG. An outburst flood from Lake Merzbacher occurs almost every year and ice from southern IG is collapsing into the lake. Thus, glacier thinning and glacier flow close to the dam was influence by Lake Merzbacher and more detailed investigations are needed to understand the influence of this lake to the glaciers mass balance besides debris cover and climate change.

Acknowledgements. This work was supported by the Ministry of Science and Technology of the People's Republic of China (Grant 2013CBA01808); State Key Laboratory of Cryospheric Sciences (SKLCS-ZZ-2012–00-02); the National Natural Science Foundation of China (Grant: 41271082 and 41030527); the CAS Strategic Priority Research Program-Climate Change: Carbon Budget and Relevant Issue (Grant No. XDA05090302), German Research Foundation (Deutsche Forschungsgemeinschaft, DFG, code BO 3199/2-1) and the German Ministry of Education and Science (BMBF: Code 01 LL 0918 B). China Scholarship Council supported the research stay of the first author at University of Zurich. We also thank the groups of Bolot Moldobekov from Central-Asia Institute for Applied Geosciences (CAIAG) for supporting our field work in 2010 and 2012. ASTER GDEM and SRTM is a product of METI and NASA. We thanks DLR for allowing free access to SRTM X-band data and USGS for SRTM C-band data, Landsat archive.

References

Aizen, V. B., Aizen, E. M., Melack, J. M., and Dozier, J.: Climatic and Hydrologic Changes in the Tien Shan, Central Asia, J. Climate, 10, 1393–1404, 1997.

Aizen, V. B., Kuzmichenok, V. A., Surazakov, A. B., and Aizen, E. M.: Glacier changes in the central and northern Tien Shan during the last 140 years based on surface and remote-sensing data, Ann. Glaciol., 43, 202–213, 2006.

Aizen, V. B., Aizen, E. M., and Kuzmichonok, V. A.: Glaciers and hydrological changes in the Tien Shan: simulation and prediction, Environ. Res. Lett., 2, 045019, doi:10.1088/1748-9326/2/4/045019, 2007.

Benn, D. I., Bolch, T., Hands, K., Gulley, J., Luckman, A., Nicholson, L. I., Quincey, D., Thompson, S., Toumi, R., and Wiseman, S.: Response of debris-covered glaciers in the Mount Everest region to recent warming, and implications for outburst flood hazards, Earth-Sci. Rev., 114, 156–174, doi:10.1016/j.earscirev.2012.03.008, 2012.

Berthier, E., Arnaud, Y., Kumar, R., Ahmad, S., Wagnon, P., and Chevallier, P.: Remote sensing estimates of glacier mass balances in the Himachal Pradesh (Western Himalaya, India), Remote Sens. Environ., 108, 327–338, doi:10.1016/j.rse.2006.11.017, 2007.

Berthier, E., Schiefer, E., Clarke, G. K. C., Menounos, B., and Remy, F.: Contribution of Alaskan glaciers to sea-level rise derived from satellite imagery, Nat. Geosci., 3, 92–95, doi:10.1038/NGEO737, 2010.

Bolch, T.: Climate change and glacier retreat in northern Tien Shan (Kazakhstan/Kyrgyzstan) using remote sensing data, Glob. Planet. Change, 56, 1–12, 2007.

Bolch, T., Buchroithner, M., Pieczonka, T., and Kunert, A.: Planimetric and volumetric glacier changes in the Khumbu Himal, Nepal, since 1962 using Corona, Landsat TM and ASTER data, J. Glaciol., 54, 592–600, doi:10.3189/002214308786570782, 2008.

Bolch, T., Menounos, B., and Wheate, R.: Landsat-based inventory of glaciers in western Canada, 1985–2005, Remote Sens. Environ., 114, 127–137, 2010.

Bolch, T., Pieczonka, T., and Benn, D. I.: Multi-decadal mass loss of glaciers in the Everest area (Nepal Himalaya) derived from stereo imagery, The Cryosphere, 5, 349–358, doi:10.5194/tc-5-349-2011, 2011.

Bouillon, A., Bernard, M., Gigord, P., Orsoni, A., Rudowski, V., and Baudoin, A.: SPOT 5 HRS geometric performances: using block adjustment as a key issue to improve quality of DEM generation, ISPRS J. Photogramm., 60, 134–146, doi:10.1016/j.isprsjprs.2006.03.002, 2006.

Cuffey, K. and Paterson, W. S. B.: The Physics of Glaciers, 4rd edn., Elsevier Sci., New York, 704 pp., 2010.

Ding, Y., Liu, S., Li, J., and Shangguan, D.: The retreat of glaciers in response to recent climate warming in western China, Ann. Glaciol., 43, 97–105, 2006.
Gardelle, J., Berthier, E., Arnaud, Y., and Kääb, A.: Region-wide glacier mass balances over the Pamir-Karakoram-Himalaya during 1999–2011, The Cryosphere, 7, 1263–1286, doi:10.5194/tc-7-1263-2013, 2013.
Gardner, A. S., Moholdt, G., Cogley, J. G., Wouters, B., Arendt, A. A., Wahr, J., Berthier, E., Hock, R., Pfeffer, W. T., Kaser, G., Ligtenberg, S. R. M., Bolch, T., Sharp, M. J., Hagen, J. O., van den Broeke, M. R., and Paul, F.: A reconciled estimate of glacier contributions to sea level rise: 2003 to 2009, Science, 340, 852–857, doi:10.1126/science.1234532, 2013.
Glazirin, G. E.: A century of investigations on outbursts of the ice-dammed lake Merzbacher (central Tien Shan), Austrian Journal of Earth Sciences, 103, 171–178, 2010.
Gorokhovich, Y. and Voustianiouk, A.: Accuracy assessment of the processed SRTM-based elevation data by CGIAR using field data from USA and Thailand and its relation to the terrain characteristics, Remote Sens. Environ., 104, 409–415, doi:10.1016/j.rse.2006.05.012, 2006.
Hagg, W., Mayer, C., Lambrecht, A., and Helm, A.: Sub-debris melt rates on southern Inylchek Glacier, Central Tian Shan., Geogr. Ann. A, 90, 55–63, 2008.
Han, H., Wang, J., Wei, J., and Liu, S.: Backwasting rate on debris-covered Koxkar glacier, Tuomuer mountain, China, J. Glaciol., 56, 287–296, doi:10.3189/002214310791968430, 2010.
Hausler, H., Scheibz, J., Leber, B., Kopecny, A., Echtler, H., Wetzel, H.-U., and Moldobekov, B.: Results from the 2009 geoscientific expedition to the Inylchek glacier, Central Tien Shan (Kyrgyzstan), Austrian Journal of Earth Sciences, 104, 47–57, 2011.
Hodgkins, R., Fox, A., and Nuttall, A.-M.: Geometry change between 1990 and 2003 at Finsterwalderbreen a Svalbard surge-type glacier, from GPS profiling, Ann. Glaciol., 46, 131–135, 2007.
Huss, M.: Density assumptions for converting geodetic glacier volume change to mass change, The Cryosphere, 7, 877–887, doi:10.5194/tc-7-877-2013, 2013.
Jacob, T., Wahr, J., Pfeffer, W. T., and Swenson, S.: Recent contributions of glaciers and ice caps to sea level rise, Nature, 482, 514–518, doi:10.1038/nature10847, 2012.
Leprince, S., Barbot, S., Ayoub, F., and Avouac, J. P.: Automatic and precise orthorectification, coregistration, and subpixel correlation of satellite images, application to ground deformation measurements, IEEE T. Geosci. Remote, 45, 1529–1558, 2007.

Li Jia, L. Z.-W., Wang, C.-C., Zhu, J.-J., and Ding, X.-L.: Using SAR offset-tracking approach to estimate surface motion of the South Inylchek Glacier in Tianshan, Chinese J. Geophys., 56, 1226–1236, 2013.
Li, X., Cheng, G., Jin, H., Kang, E., Che, T., Jin, R., Wu, L., Nan, Z., Wang, J., and Shen, Y.: Cryospheric change in China, Glob. Planet. Change, 62, 210–218, doi:10.1016/j.gloplacha.2008.02.001, 2008.
Liu, S. Y., Ding, Y. J., Shangguan, D. H., Zhang, Y., Li, J., Han, H. D., Wang, J., and Xie, C. W.: Glacier retreat as a result of climate warming and increased precipitation in the Tarim river basin, northwest China, Ann. Glaciol., 43, 91–96, 2006.
Mayer, C., Hagg, W., Lambrecht, A., Helm, A. and Scharrer, K.: Post-drainage ice dam response at Lake Merzbacher, Inylchek glacier, Kyrgyzstan, Geograf. Ann., 90, 87–96, 2008.
Narama, C., Kääb, A., Duishonakunov, M., and Abdrakhmatov, K.: Spatial variability of recent glacier area changes in the Tien Shan Mountains, Central Asia, using Corona (~ 1970), Landsat (~ 2000), and ALOS (~ 2007) satellite data, Glob. Planet. Change, 71, 42–54, doi:10.1016/j.gloplacha.2009.08.002, 2010.
Ng, F., Liu, S., Mavlyudov, B., and Wang, Y.: Climateic control on the peak discharge of glacier outburst floods, Geophys. Res. Lett., 34, L21503, doi:10.1029/2007GL031426, 2007.
Nobakht, M., Motagh, M., Wetzel, H.-U., Roessner, S., and Kaufmann, H.: The Inylchek Glacier in Kyrgyzstan, Central Asia: insight on surface kinematics from optical remote sensing imagery, Remote Sensing, 6, 841–856, 2014.
Nuimura, T., Fujita, K., Yamaguchi, S., and Sharma, R. R.: Elevation changes of glaciers revealed by multitemporal digital elevation models calibrated by GPS survey in the Khumbu region, Nepal Himalaya, 1992–2008, J. Glaciol., 58, 648–656, doi:10.3189/2012JoG11J061, 2012.
Nuth, C. and Kääb, A.: Co-registration and bias corrections of satellite elevation data sets for quantifying glacier thickness change, The Cryosphere, 5, 271–290, doi:10.5194/tc-5-271-2011, 2011.
Osmonov, A., Bolch, T., Xi, C., Kurban, A., and Guo, W.: Glacier characteristics and changes in the Sary-Jaz River Basin (Central Tien Shan, Kyrgyzstan) – 1990–2010, Remote Sensing Letters, 4, 725–734, doi:10.1080/2150704x.2013.789146, 2013.
Paul, F. and Haeberli, W.: Spatial variability of glacier elevation changes in the Swiss Alps obtained from two digital elevation models, Geophys. Res. Lett., 35, L21512, doi:10.1029/2008gl034718, 2008.

Paul, F., Kääb, A., Maisch, M., Kellenberger, T., and Haeberli, W.: Rapid disintegration of Alpine glaciers observed with satellite data, Geophys. Res. Lett., 31, L21402, doi:10.1029/2004gl020816, 2004.
Paul, F., Barrand, N. E., Berthier, E., Bolch, T., Casey, K., Frey, H., Joshi, S. P., Konovalov, V., Bris, P. L., Molg, N., NOsenko, G., Nuth, C., Pope, A., Racoviteanu, A., Rastner, P., Raup, B., and Scharrer, K.: On the accuracy of glacier outlines derived from remote-sensing data, Ann. Glaciol., 54, 171–182, doi:10.3189/2013AoG63A296, 2013.
Paul, F., Bolch, T., Kääb, A., Nagler, T., Nuth, C., Scharrer, K., Shepherd, A., Strozzi, T., Ticconi, F., Bhambri, R., Berthier, E., Bevan, S., Gourmelen, N., Heid, T., Jeong, S., Kunz, M., Lauknes, T. R., Luckman, A., Merryman, J., Moholdt, G., Muir, A., Neelmeijer, J., Rankl, M., VanLooy, J., and Van Niel, T.: The glaciers climate change initiative: methods for creating glacier area, elevation change and velocity products, Remote Sens. Environ., in press, doi:10.1016/j.rse.2013.07.043, 2014.
Piao, S., Ciais, P., Huang, Y., Shen, Z., Peng, S., Li, J., Zhou, L., Liu, H., Ma, Y., Ding, Y., Friedlingstein, P., Liu, C., Tan, K., Yu, Y., Zhang, T., and Fang, J.: The impacts of climate change on water resources and agriculture in China, Nature, 467, 43–51, doi:10.1038/nature09364, 2010.
Pieczonka, T., Bolch, T., Junfeng, W., and Shiyin, L.: Heterogeneous mass loss of glaciers in the Aksu-Tarim Catchment (Central Tien Shan) revealed by 1976 KH-9 Hexagon and 2009 SPOT-5 stereo imagery, Remote Sens. Environ., 130, 233–244, 2013.
Pressel, P.: Meeting the Challenge: The Hexagon KH-9 Reconnaissance Satellite, American Institute of Aeronautics and Astronautics, Inc., Reston, Virginia, 2013.
Quincey, D. J., Copland, L., Mayer, C., Bishop, M., Luckman, A., and Belo, M.: Ice velocity and climate variations for Baltora Glacier, Pakistan, J. Glaciol., 55, 1061–1071, 2009.
Reyers, M., Pinto, J. G., and Paeth, H.: Statistical–dynamical downscaling of present day and future precipitation regimes in the Aksu river catchment in Central Asia, Glob. Planet. Change, 107, 36–49, doi:10.1016/j.gloplacha.2013.04.003, 2013.
Rignot, E., Echelmeyer, K., and Krabill, W.: Penetration depth of interferometric synthetic-aperture radar signals in snow and ice, Geophys. Res. Lett., 28, 3501–3504, doi:10.1029/2000gl012484, 2001.
Schomacker, A.: What controls dead-ice melting under different climate conditions? a discussion, Earth-Sci. Rev., 90, 103–113, 2008.

Shen, Y. P., Wang, G. Y., Ding, Y. J., Mao, W. Y., Liu, S. Y., Wang, S. D., and Mamatkanov, D. M.: Changes in glacier mass balance in watershed of sary Jaz-Kumarik Rivers of Tianshan Mountains in 1957–2006 and their impact on water resources and trend to end of the 21th century, J. Glaciol. Geocryol., 31, 792–801, 2009 (in Chinese with English abstract).
Shortridge, A. and Messina, J.: Spatial structure and landscape associations of SRTM error, Remote Sens. Environ., 115, 1576–1587, doi:10.1016/j.rse.2011.02.017, 2011.
Shukla, A., Arora, M. K., and Gupta, R. P.: Synergistic approach for mapping debris-covered glaciers using optical-thermal remote sensing data with inputs from geomorphometric parameters, Remote Sens. Environ., 114, 1378–1387, 2010.
Sorg, A., Bolch, T., Stoffel, M., Solomina, O., and Beniston, M.: Climate change impacts on glaciers and runoff in Tien Shan (Central Asia), Nature Climate Change, 2, 725–731, doi:10.1038/nclimate1592, 2012.
State Bureau of Surveying and Mapping (SBSM): Technical rules for producing digital products of 1 : 10 000 1 : 50 000 fundamental geographic information, CH/T 1015.1-2007, State Bureau of Surveying and Mapping, Beijing, 2007.
Takaku, J., Futamura, N., Iijima, T., Tadono, T., Shimada, M., and Shibasaki, R.: High resolution DEM generation from ALOS PRISM data – simulation and evaluation, Geoscience and Remote Sensing Symposium, 2004. IGARSS '04. Proceedings 2004, IEEE International, vol. 4547, 4548–4551, 20–24 September 2004.
Toutin, T.: Generation of DSMs from SPOT-5 in-track HRS and across-track HRG stereo data using spatiotriangulation and autocalibration, ISPRS J. Photogramm., 60, 170–181, doi:10.1016/j.isprsjprs.2006.02.003, 2006.
Uchiyama, Y., Honda, M., Mizuta, Y., Otsuka, K., Ishizeki, T., Okatani, T., and Tamura, E.: Revising 1 : 25 000-Scale topographic maps using ALOS/PRISM Imagery, Bulletin of the Geographical Survey Institute, 56, 1–15, 2008.
USGS: Shuttle Radar Topography Mission, 3 Arc Second scene, Unfilled finished B, Global Land Cover Facility, University of Maryland, College Park, Maryland, February 2000, 2006.
WGMS: Fluctuations of Glaciers Database, World Glacier Monitoring Service, Zurich, Switzerland, doi:10.5904/wgms-fog-2013-11, 2013.
Xu, J., Liu, S., Zhang, S., Guo, W., and Wang, J.: Recent changes in glacial area and volume on Tuanjiefeng Peak region of Qilian Mountains, China, PLoS ONE, 8, e70574, doi:10.1371/journal.pone.0070574, 2013.

Yang, L., Meng, X., and Zhang, X.: SRTM DEM and its application advances, Int. J. Remote Sens., 32, 3875–3896, doi:10.1080/01431161003786016, 2011.

Table 1. List of applied satellite images and data sources.

Satellite	Time	Pixel size (nadir, m)	Swatch (km)	B/H	DEM pixel size (m)	Velocity image
ALOS Nadir (N) Backwards(B)	8 Oct, 2006	2.5	35	0.5	10	–
SPOT5 HRG	5 Feb 2008	2.5	60	0.63	10	–
SRTM Unfilled Finished-B version	Feb, 2000		$1^{\circ} \times 1^{\circ}$ (tile size)	–	90	–
Landsat ETM+	13 Oct 1999	15	185	–	–	–
Landsat TM	10 Sep 1990	30	185	–	–	–
KH9-Hexagon	16 Nov 1974	6–9	240 × 120		25	–
Terra ASTER	25 Aug 2002	15	60			Yes
Terra ASTER	28 Aug 2003	15	60			Yes
Landsat TM	16 Aug 2010	30	185			Yes
Landsat TM	3 Aug 2011	30	185			Yes

Table 2. RMSE for GCPs of ALOS and SPOT5 data.

	ALOS	SPOT5
No.GCPs	4	4
RMSEx	0.99 m	1.4 m
RMSEy	2.15 m	1.3 m
RMSEz	1.5 m	2.5 m

Table 3. Shift vectors in x, y and z direction and DEM uncertainty.

	Shift vectors in x, y and z direction			Before co-registration with glacier free		After co-registation		Normalized median absolute deviation (m)	Uncertainty (m)
	X (m)	Y (m)	Z (m)	Mean elevation difference (m)	Standard deviation (STD) (m)	Mean elevation difference (m)	Standard deviation (m)		
SRTM-> SPOT	18.7	−46.5	1.3	6.8	20.8	0.4	13.0	1.0	2.1
SRTM-> KH9	34.3	27.3	−5.3	−2.0	18.1	−1.0	15.3	0.5	2.0
SPOT-> KH9	−3.8	22.4	−6.3	−7.7	15.9	−1.4	15.9	1.1	1.1
SRTM-> ALOS	23.5	−51.2	6	−6.5	22.3	2.5	10.1	2.1	2.8
ALOS-> KH9	6.2	22.8	−19.5	−12.8	20.5	2.7	19.0	2.3	2.3

Table 4. Comparison with GPS and DEMs before and after co-registration.

			In stu	DEMs Before co-registration				Difference	After co-registration		Description
No	Latitude	Longitude	GPS_Elevation (m)	SPOT_DEM (m)	ALOS_DEM (m)	SRTM_DEM (m)	KH9 (m)	GPS_SPOT (m)	SPOT_DEM (m)	GPS_SPOT (m)	
1	42.22421	79.85953	3351.5	3342.9	3334.0	3454	3329.2	8.6	3350.7	0.8	Glacier free region
2	42.16847	49.8211	3372.4	3358.4	3365.1	3372	3387.1	14.0	3370.7	1.7	Glacier free region
3	42.21839	79.85553	3303.0	3287.0	3298.4	3299	3302.8	16	3299.4	3.6	Debris covered region
4	42.20931	79.84357	3306.3	3287.0	3286.6	3297	3281.6	9.3	3306.2	0.1	Debris covered region
5	42.22095	79.86032	3294.1	3295.0	3296.5	3304	3289.0	−0.94	3305.9	−11.8	Debris covered region
6	42.17129	79.84033	3430.6	3428.4	3418.5	3433	3451.7	2.2	3427.6	3.0	Glacier region

Table 5. The Southern IG and Northern IG area change betweeen 1974 and 2007.

	Area (km^2)				Area change							
	1974	1990	1999	2007	1974–1990		1990–1999		1999–2007		1974–2007	
					km^2	%	km^2	%	km^2	%	km^2	%
Southern IG	508.4 ± 6.6	508.3 ± 9.7	507.8 ± 4.6	507.6 ± 2.5	−0.1 ± 0.1	–	−0.5 ± 0.0	−0.1	−0.2 ± 0.0	–	−0.8 ± 0.0	−0.2
Northern IG	156.6 ± 2.8	155.3 ± 4.2	159.0 ± 2.1	158.6 ± 0.5	−1.2 ± 0.1	−0.8	3.7 ± 0.3	2.4	−0.4 ± 0.1	−0.3	2.0 ± 0.1	1.3
Total	664.9 ± 7.2	663.6 ± 10.6	666.9 ± 5.1	666.2 ± 2.5	−1.3 ± 0.1	0.2	3.2 ± 0.2	0.5	−0.7 ± 0.1	−0.1	1.3 ± 0.1	0.2

Table 6. Glacier surface change for period 1974–2007.

		Observation region (km^2)	Percentage of total area (%)	Glacier surface change ($m\,a^{-1}$)
IG	SPOT-SRTM	224.7	33.7	0.5 ± 0.5
	SRTM-KH9	136.4	20.5	-0.8 ± 0.1
	SPOT-KH9	115.1	17.3	-0.5 ± 0.1
North IG	SPOT-SRTM	34.3	21.6	-0.2 ± 0.5
	SRTM-KH9	16.6	10.4	0.7 ± 0.1
	SPOT-KH9	14.1	8.9	0.1 ± 0.1
South IG	SPOT-SRTM	190.5	37.5	0.5 ± 0.5
	SRTM-KH9	119.8	23.6	-1.1 ± 0.1
	SPOT-KH9	101.0	19.9	-0.7 ± 0.1

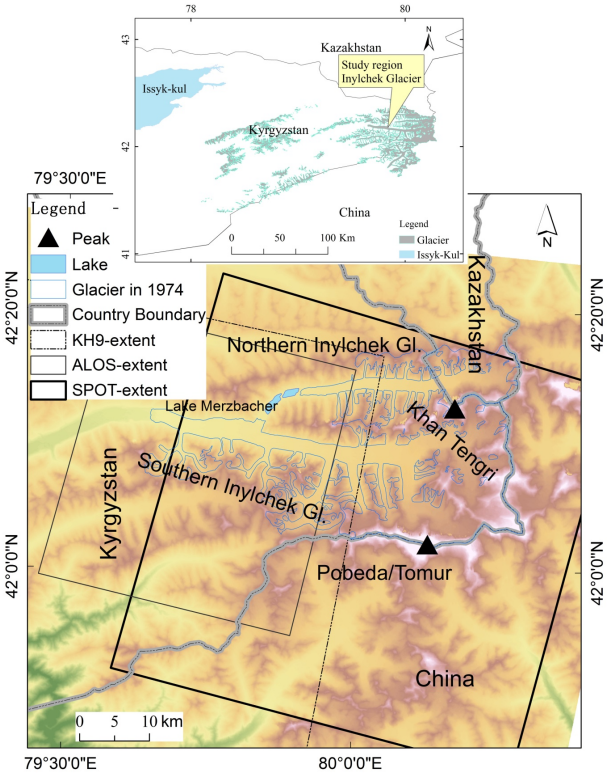

Figure 1. Location and topography of the Inylchek Glacier.

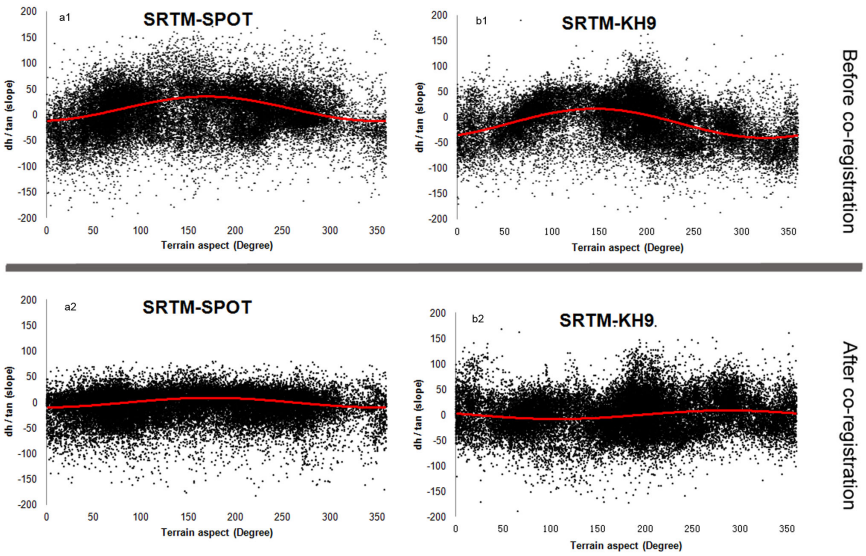

Figure 2. Scatter plot of slope standardized elevation differences of Terrain aspect. **(a1)** SRTM vs. SPOT5 before co-registration; **(a2)** SRTM vs. SPOT5 after co-registration; **(b1)** SRTM vs. KH9 before co-registration; **(b2)** SRTM vs. KH9 after co-registration.

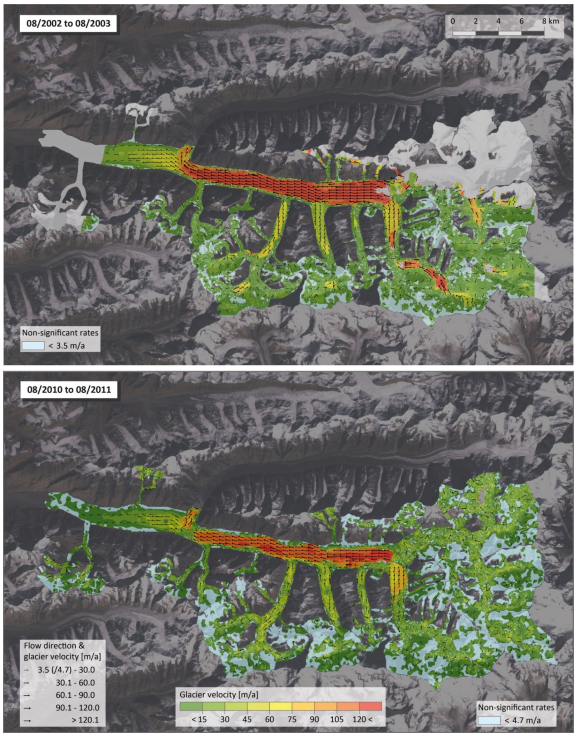

Figure 3. Flow direction and velocity of southern IG [m a^{-1}] between 2002 and 2003 (above) and 2010 and 2011 (below).

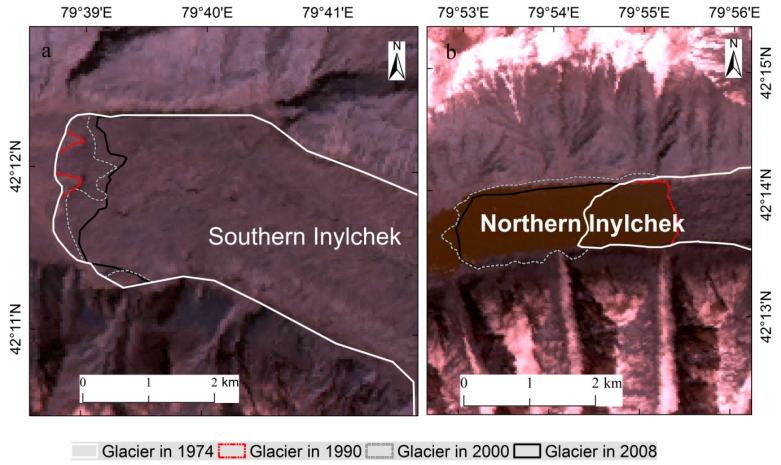

Figure 4. The Southern IG and Northern IG change between 1974 and 2007. The background Landsat TM image was acquired in 1990.

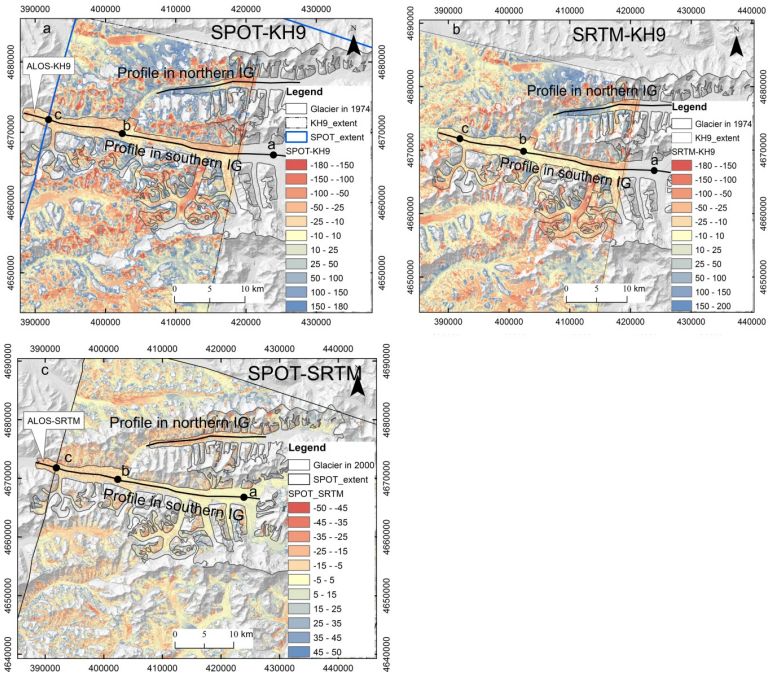

Figure 5. (a) Elevation difference of IG between SPOT (2007) and KH9 (1974); **(b)** elevation difference of IG between SRTM (1999) and KH9 (1974); **(c)** elevation difference of IG between SPOT5 (2007) and SRTM (1999). Point a, point b and point c are three reference points. The altitude of point a, point b and point c is ~ 4000 m a.s.l., ~ 3380 m a.s.l. and ~ 3070 m a.s.l. derived from SRTM. Point c is on the boundary of SPOT DEM. From the tongue of southern IG to point c, the ice elevation differences were derived from ALOS-KH9 in Fig. 4a and ALOS-SRTM in Fig. 4c.

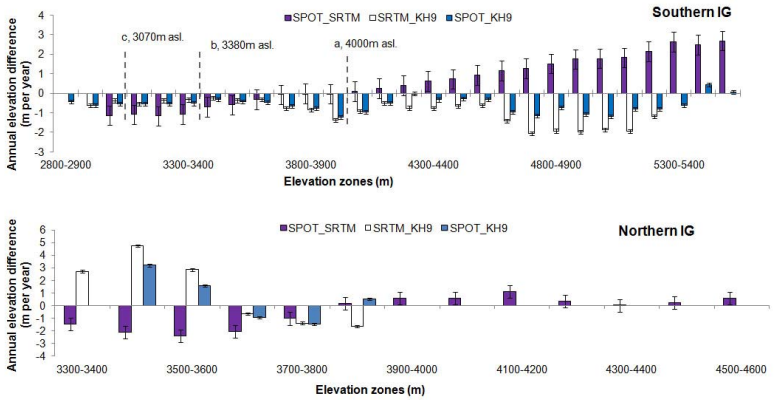

Figure 6. The average annual change in glacier elevation measured for the period of 1974–1999, 1999–2007 and 1974–2007 along the altitude zone in the southern IG and northern IG. In southern IG, the annual change in zone 2800–3000 was derived from ALOS-KH9 between 1974–2006.

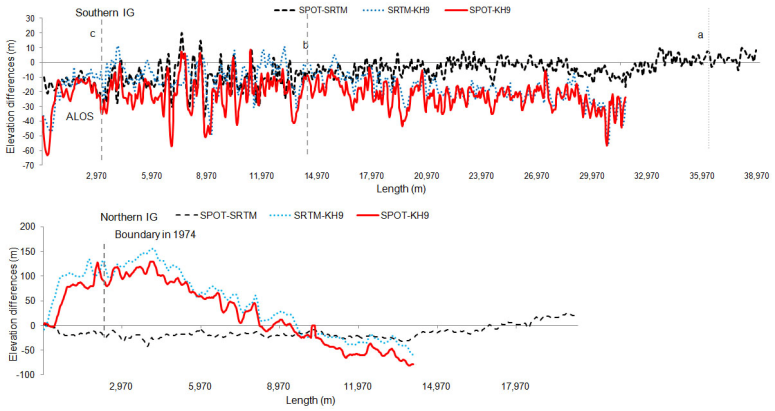

Figure 7. Longitudinal profile of northern IG and southern IG for the period 1974–1999, 1999–2007 and 1974–2007. And the section of ALOS between the tongue of southern IG and point a was derived from ALOS-SRTM in black line and was derived from ALOS-KH9 in red line.